

The spread of the gluon k_t -distribution and the determination of the saturation scale at hadron colliders in resummed NLL BFKL

V.A. KHOZE^{a,b}, A.D. MARTIN^a, M.G. RYSKIN^{a,b} AND W.J. STIRLING^{a,c}

^a Department of Physics and Institute for Particle Physics Phenomenology,
University of Durham, DH1 3LE, UK

^b Petersburg Nuclear Physics Institute, Gatchina, St. Petersburg, 188300, Russia

^c Department of Mathematical Sciences, University of Durham, DH1 3LE, UK

Abstract

The transverse momentum distribution of soft hadrons and jets that accompany central hard-scattering production at hadron colliders is of great importance, since it has a direct bearing on the ability to separate new physics signals from Standard Model backgrounds. We compare the predictions for the gluonic k_t -distribution using two different approaches: resummed NLL BFKL and DGLAP evolution. We find that as long as the initial and final virtualities (k_t) along the emission chain are not too close to each other, the NLL resummed BFKL results do not differ significantly from those obtained using standard DGLAP evolution. The saturation momentum $Q_s(x)$, calculated within the resummed BFKL approach, grows with $1/x$ even slower than in the leading-order DGLAP case.

1 Introduction

The high-energy behaviour of QCD amplitudes is described by the BFKL/CCFM equation [1, 2] which sums to all orders leading logarithmic contributions of the form $(\alpha_s \ln s)^n$. The next-to-leading logarithmic (NLL) corrections $\alpha_s(\alpha_s \ln s)^n$ have been calculated in Refs. [3]. The NLL corrections turn out to have a large numerical effect, and therefore in order to obtain reliable predictions one needs to first understand the origin of the large numerical coefficients at NLL and then if possible to further resum the main part of the NLL contribution.

In the past few years there have been a number of studies of the BFKL approach at NLL accuracy, see Refs. [4, 5, 6], which concentrate on the properties and the behaviour of the gluon Green function. In this paper we focus instead on the gluon transverse momentum (k_t) distribution along the BFKL evolution chain and compare the predictions obtained using both the resummed NLL BFKL and the LO DGLAP evolution approaches.

Besides the pure theoretical interest in further understanding the properties of QCD in the high-energy limit, there are also important phenomenological implications. Precise knowledge of the k_t distribution of intermediate (i.e. accompanying) gluons is important for achieving a better understanding of the structure of the so-called ‘underlying event’ at hadron colliders such as the Tevatron and the LHC. As has been emphasized in [7], the fact that the transverse momentum of the emitted partons (and therefore of the soft hadrons and minijets) grows with energy (i.e. with $1/x$) could cause problems due to a ‘noisy’ underlying event affecting the extraction of a clean new-physics signal (for example, inclusive production of Higgs bosons, SUSY particles, etc.) at the LHC. Therefore it is very important to be able calculate the predicted gluon k_t distribution as precisely as possible. Of course the standard approach is to use parton shower Monte Carlos such as HERWIG and PYTHIA to estimate the k_t distribution of accompanying partons/hadrons. However as these models are based on DGLAP evolution, they do *not* contain all the expected logarithmic contributions in the high-energy limit. It is therefore important to understand how and why the DGLAP and (potentially more realistic) resummed NLL BFKL approaches differ. Such a comparison will form a major part of our study. Also very relevant, is the high-energy behaviour of the saturation momentum Q_s — the transverse momentum at which non-linear effects (from gluon-gluon rescattering and recombination) become important and start to saturate the parton densities.

The BFKL amplitude is usually described in terms of the Pomeron intercept (i.e. the singularity in the complex momentum j -plane) $j = 1 + \omega(\gamma)$ which depends on the anomalous dimension (γ) of the eigenfunction. In contrast, DGLAP evolution is usually described in terms of $\gamma(\omega)$, i.e. the anomalous dimension is considered as a function of ω , the conjugate variable to x .

In order to compare the DGLAP and BFKL predictions, in Section 2 we will consider the unintegrated gluon distribution $f_g(x, k_t, \mu)$ — that is, the probability to find a gluon carrying longitudinal momentum fraction x and transverse momentum k_t in a process with (hard) factorization scale μ — written in the form of a double contour integral over both γ and ω , i.e. performing simultaneous Mellin transforms with respect to both the k_t and x distributions. Depending on which of these integrations is performed first, one obtains either the standard DGLAP or the BFKL form.

In Section 3 we introduce a resummation which is a modification of that proposed by the Firenze group [8, 9]. The idea is to modify the contribution of the poles at $\gamma = 0$ ($\gamma = 1$) corresponding to the normal (inverse) k_t -ordered DGLAP evolution. To be explicit, we include the full LO DGLAP (splitting function) contribution, allow for the appropriate ‘energy’ variable $x = Q^2/s$, and account for energy-momentum conservation. After these modifications have been made, it has been shown that the remaining part of the NLL correction does not exceed 7% of the original value.

Solving the BFKL equation for the intercept

$$j = 1 + \omega(\gamma) = 1 + \frac{\alpha_s N_c}{\pi} \chi(\gamma) \quad (1)$$

with respect to γ , one obtains the NLO contribution $C_n(\alpha_s/\omega)^{n+1}$ to the DGLAP anomalous dimension $\gamma(\omega)$, equivalently the $C_n x^{-1} \alpha_s^n \ln^{n-1}(x)$ contribution to the (gluon-gluon) splitting function. It turns out that in leading-order (LO) BFKL the first two non-trivial terms vanish¹, i.e. $C_1 = C_2 = 0$ [10]. Therefore the expected BFKL corrections to DGLAP evolution are numerically rather weak (see [11] for a more detail discussion). On the other hand, in terms of the intercept j the value of $\omega(\gamma)$ given by the LO BFKL equation is much larger than that coming from DGLAP. At first sight this looks like a contradiction. However the situation changes dramatically after the NLL resummation. Now the BFKL intercept becomes close to, and even slightly smaller than, the corresponding DGLAP quantity. Thus in any kinematic configuration where the initial and final virtualities (transverse momenta) are not too close to each other, the DGLAP and the BFKL predictions do not differ significantly (in agreement with the conclusions of Ref. [11]).

The dependence of the k_t distribution on the overall event kinematics is discussed in Section 4 and the x -dependence of the saturation momentum $Q_s(x)$ is discussed in Section 5. Section 6 contains our conclusions.

2 The unintegrated gluon distribution

We begin by considering the unintegrated (over transverse momentum) gluon distribution $f_g(x, k_t, \mu)$, in the form [12]

$$f_g(x, k_t, \mu) = T_g(k_t, \mu) \frac{\alpha_s(k_t^2)}{2\pi} \int_x^{1-\Delta} dz P_{gg}(z) (x/z) g(x/z, k_t^2) \quad (2)$$

where the survival probability T is given by

$$T_g(k_t, \mu) = \exp \left(- \int_{k_t^2}^{\mu^2} \frac{dk_t'^2}{k_t'^2} \frac{\alpha_s(k_t'^2)}{2\pi} \int_0^1 dz' \left(\Theta(z' - \Delta) \Theta(1 - z' - \Delta) z' P_{gg}(z') + n_F P_{qg}(z') \right) \right). \quad (3)$$

Here the infrared cutoff is $\Delta = k_t/(\mu + k_t)$; μ is the factorisation scale; and n_F is the number of active quark flavours. When k_t is close to μ we may neglect the double logarithms in the

¹Note that Eq. (6) below can be written in the form $X_0 = 1/\gamma + 2\Psi(0) - \Psi(1+\gamma) - \Psi(1-\gamma) = 1/\gamma + O(\gamma^2)$.

T -factor, since $\alpha_s \ln^2(k_t/\mu) \ll 1$, and thus $T \simeq 1$. Then the unintegrated distribution is simply related to the derivative of the standard (integrated) gluon parton distribution function:

$$f_g(x, k_t) = \left[\frac{d}{d \ln \mu^2} xg(x, \mu^2) \right]_{\mu=k_t}. \quad (4)$$

Introducing the Mellin-transform variables, γ and ω , conjugate to k_t^2 and $1/x$ respectively, we can write f_g as

$$f_g(x, k_t) = \int_{-i\infty}^{+i\infty} \frac{d\gamma}{2\pi i} \int_{-i\infty}^{+i\infty} \frac{d\omega}{2\pi i} F(\gamma, \omega) \frac{e^{\omega Y + \gamma r}}{\omega - \bar{a}X(\gamma, \omega)} \quad (5)$$

where $\bar{a} = N_c \alpha_s / \pi$, $Y = \ln(1/x)$ and $r = \ln(k_t^2/Q_0^2)$. $F(\gamma, \omega)$ represents the input distribution at $k_t^2 = Q_0^2$, where Q_0 is the starting scale for perturbative evolution assumed to be ~ 1 GeV. X is the resummed BFKL intercept, $X = X_0 + \bar{a}X_1$, where the leading order (LL) contribution is

$$X_0(\gamma) = 2\Psi(1) - \Psi(\gamma) - \Psi(1 - \gamma) \quad (6)$$

and X_1 is the NLL correction. The contour integration over ω goes to the right of all singularities, while the real part of the anomalous dimension γ is bounded by $0 < \text{Re}\gamma < 1$.

In the DGLAP limit $r \gg Y$ we close the γ contour around the pole given by $1/(\omega - \bar{a}X)$, leaving the inverse Mellin integral over ω with $\gamma = \gamma(\omega)$. In the BFKL case ($Y \gg r$) we close the ω contour around the same pole $1/(\omega - \bar{a}X)$ and write the result as an integral over γ , with $\omega = \omega(\gamma)$. In the latter form

$$f_g = \int_{-i\infty}^{+i\infty} \frac{d\gamma}{2\pi i} e^{\gamma r + \omega_s Y} B(\gamma) \quad (7)$$

with $\omega_s(\gamma)$ given by the solution of the equation

$$\omega - \bar{a}X(\gamma, \omega) = 0 \quad (8)$$

and

$$B(\gamma) = \frac{F(\gamma, \omega_s(\gamma))}{1 - X'_\omega}, \quad X'_\omega = \left. \frac{\partial X(\gamma, \omega)}{\partial \omega} \right|_{\omega=\omega_s(\gamma)}. \quad (9)$$

With this representation, the input distribution at Q_0 is absorbed into $B(\gamma)$, which may therefore be fitted to reproduce the data.

Another possibility is to use the conventional Mellin (ω) representation for f_g by closing the γ contour around the nearest pole. Strictly speaking the BFKL function X_0 of Eq. (6) has poles at each integer γ . The pole at $\gamma = 0$ corresponds to the normal twist-2 DGLAP contribution, the pole at $\gamma = 1$ corresponds to inverse k_t ordering ($k_t \ll Q_0$). The other poles at $\gamma = -1, -2, \dots$ ($\gamma = 2, 3, \dots$) are the higher-twist contributions (3, 4, ... gluons in the t -channel), corresponding to normal (inverse) k_t ordering, hidden in the Reggeization of the BFKL gluons. However in practice we know that the higher-twist contribution at small x is small (see, for example, Ref. [13]). Therefore, to begin, we may neglect the poles at negative γ , arguing that phenomenologically the input function $F(\gamma, \omega)$ is numerically small at negative

integer values of γ .² We then obtain

$$f_g = \int_{-i\infty}^{+i\infty} \frac{d\omega}{2\pi i} e^{\gamma_s(\omega)r + \omega Y} D(\omega) \quad (10)$$

where

$$D(\omega) = \gamma_s(\omega) M(\omega) \quad (11)$$

and $M(\omega) = \int_0^1 x^\omega g(x, Q_0^2) dx$ is the known Mellin transform (x -moments) of the input gluon distribution. The first factor γ in (11) is due to the derivative in (4), and all γ dependent quantities are evaluated at $\gamma = \gamma_s(\omega)$, the solution of (8).

3 The resummed NLL BFKL intercept

In this section we consider the resummed NLL contribution to the unintegrated gluon distribution defined in the previous section. We use the idea proposed in Ref. [9], but with a small modification, which is rather simple and more convenient for our purpose. The crucial point is the fact that the major part of the $O(\alpha_s)$ correction is actually contained in the $O(\omega)$ contribution³. Next we note that the nearest, and most important, poles in the quantity X of Eq. (6) at $\gamma = 0$ and $\gamma = 1$ correspond, respectively, to the well known, normal- ($k_t \gg Q_0$) and inverted- ($k_t \ll Q_0$) ordered, twist-2 DGLAP contributions. Thus the leading-order characteristic function X_0 contains two parts. One is the twist-2 poles $1/\gamma$ and $1/(1-\gamma)$, and the remainder is the higher-twist component, $X_0^{(\text{ht})}$. That is

$$X_0 = \frac{1}{\gamma} + \frac{1}{1-\gamma} + X_0^{(\text{ht})}, \quad (12)$$

where, from (6), we have

$$X_0^{(\text{ht})} = 2\Psi(1) - \Psi(1+\gamma) - \Psi(2-\gamma). \quad (13)$$

First, we have to modify the poles to include in the residues the *full* LO DGLAP splitting function. Because in the physical (axial) gauge both the BFKL and DGLAP LO contributions are given by ladder-type Feynman diagrams, the Mellin transform of the final (modified) amplitude in the ω, γ representation may be written in the same exponential form as Eqs. (5,7,10). Thus the residue 1 in the twist-2 DGLAP pole at $\gamma = 0$ is replaced by the full DGLAP splitting function

$$\frac{1}{2N_c} \omega P_{gg}(\omega) = 1 + \omega A_1(\omega). \quad (14)$$

In pure gluodynamics (i.e. $n_F = 0$) $A_1 = -\frac{11}{12} + O(\omega)$. To account for the quark loop contribution for $n_F \neq 0$ we have to replace A_1 by

$$A_1(\omega) + n_F \left(\frac{\bar{a}}{4N_c^2\gamma} P_{gq}(\omega) P_{qg}(\omega) - \frac{1}{3} \right), \quad (15)$$

²Analogously, in the $d\gamma$ integral (7) we cannot rule out the possibility of other singularities in the ω plane situated to the left of the leading pole at $\omega = \omega_s$. However, since in any case we cannot justify the BFKL approach for large $|\omega| \sim 1$, in the present context we only keep the leading pole in (7).

³Recall that in the BFKL approach, $\omega \sim \alpha_s$.

where the first term in the brackets corresponds to the real quark two-loop contribution⁴, as indicated by the extra α_s factor. The second term is the virtual quark loop insertion in the gluon propagator, and corresponds to the P_{qg} term in the T factor of Eq. (3). Formally, the NLL correction is represented by the leading (ω) term in A_1 . Nevertheless here we keep the full ω dependence of the LO DGLAP splitting kernels. The same procedure can be followed to modify the residue of the $1/(1-\gamma)$ pole, which corresponds to the DGLAP evolution with inverse k_t ordering.

Another modification is necessary. In order to compare the BFKL and DGLAP predictions we have to write everything in terms of the DGLAP ‘energy’ variable $x = Q^2/s$. Due to the asymmetry in the definition of the energy scales, for the normal and inverse ordered contributions, we need to correct the contribution of the $1/(1-\gamma)$ pole, and to replace $(1-\gamma)$ by $(1-\gamma+\omega)$ (see Section 3.3 and Eq. (60) of Ref. [9]) in the terms that are singular when γ is close to 1.

Putting everything together, we finally obtain the characteristic function

$$X(\gamma, \omega) = X_0 + \bar{a}X_1, \quad (16)$$

where the LL intercept X_0 is given by (6). The NLL contribution

$$\bar{a}X_1 = \left(\frac{1 + \omega A_1(\omega)}{\gamma} - \frac{1}{\gamma} + \frac{1 + \omega A_1(\omega)}{1 - \gamma + \omega} - \frac{1}{1 - \gamma} \right) - \omega X_0^{(\text{ht})}, \quad (17)$$

consists of a twist-2 part, which is shown in brackets, and a correction, $-\omega X_0^{(\text{ht})}$, to the higher-twist component (13) of X_0 , whose origin we now explain. Following Ref. [14], we have multiplied the higher-twist contribution (13) by a factor $(1-\omega)$, which effectively accounts for the kinematical constraints and provides conservation of energy and momentum. At $\omega = 1$ the whole contribution vanishes. Note that the twist-2 part already satisfies this condition, since we use the full DGLAP splitting function.

We have checked that, in the important region $0 < \gamma < 0.6$, the approximation given by Eqs. (13-17) reproduces the known exact NLL BFKL $\mathcal{O}(\alpha_s)$ result to within 7% accuracy. This is illustrated in Fig. 1. For real γ , the continuous curve in the upper plot is the result of the exact calculation of X_1/X_0 for $n_F = 0$ (Eqs. (53,54) of Ref. [9], see also Refs. [3]), whereas the dashed line comes from the approximation given by Eqs. (13-17) above. We need to know the intercept not only at the saddle point ($\text{Re } \gamma \sim 0.3 - 0.5$, depending on the kinematics), but also in a region in the complex plane around this point (with $|\text{Im } \gamma| \lesssim 0.5$). We therefore show in the lower plot of Fig. 1 the deviation, ΔX_1 , of our approximation of X_1 from the exact result[3] for various values of $\text{Im } \gamma$, normalized to the value of X_1 for $\gamma = \text{Re } \gamma$ with $\text{Im } \gamma = 0$.

Moreover, note that the approximation of Eqs. (13-17) can be used even for rather large values of α_s , since from Eq. (8) we always have $\omega_s > 0$. Note that by using the above form we are effectively expanding in ω , which here plays the role of a small parameter, rather than in the coupling α_s (i.e. \bar{a}).⁵ This is the result of resumming the NLL ($\mathcal{O}(\alpha_s)$) corrections to the leading-order BFKL/CCFM intercept.

⁴The k_t integral over the second loop, in the DGLAP approximation, generates the $1/\gamma$ pole.

⁵With the exception of the quark loop contribution, see footnote 4.

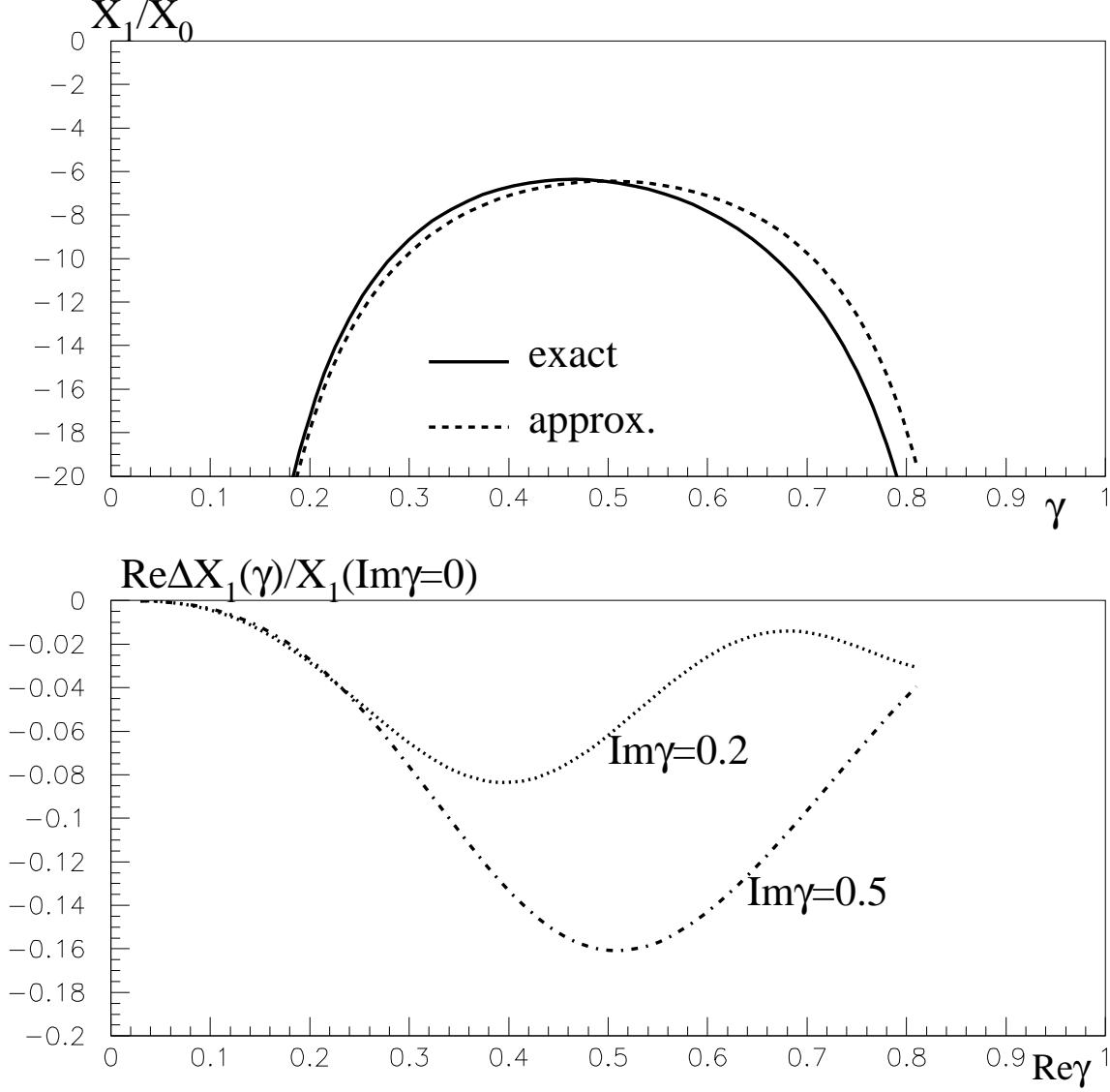


Figure 1: The comparison of the approximation of Eqs. (13-17) for the characteristic function with the exact NLL result. The upper diagram shows X_1/X_0 as a function of γ with $\text{Im } \gamma = 0$, whereas lower diagram shows the deviation, ΔX_1 , suitably normalised, of our approximation of X_1 from the exact result for various values of $\text{Im } \gamma$. Recall that $\omega = \bar{a}X_0 + \bar{a}^2X_1$, where $\bar{a} = 3\alpha_s/\pi$.

The solutions of Eq. (8) for the leading singularity $\omega_s(\gamma)$ are shown in Figs. 2 and 3. We compare the results obtained using four different approximations:

- (i) the dotted line corresponds to the well-known LO BFKL function $X(\gamma, \omega) = X_0(\gamma, 0)$;
- (ii) the Double Logarithmic (DL) contribution $X = 1/\gamma$, which is of course the same for the LO DGLAP and LO BFKL cases, is shown by the dot-dashed line;
- (iii) the solution of (8) with the full resummed function $X(\gamma, \omega)$ given by Eqs. (13-17) is shown by the solid line;
- (iv) the dashed line shows the pure DGLAP result where we keep just the same LO DGLAP contribution that was included in (17), that is $X = (1 + \omega A_1(\omega))/\gamma$.

At very small $\alpha_s = 0.01$ the solid (resummed NLL BFKL) curve is rather close to the dotted one (LO BFKL). However already at $\alpha_s = 0.15$ the NLL corrections significantly change the behaviour of ω_s for real γ (Figs. 2a,b,c and Figs. 3a,b,c). In particular, the solid (NLL BFKL) curve becomes closer to the dashed (DGLAP) curve. Note that the resummed value of ω_s depends weakly on the QCD coupling α_s . The NLL BFKL solutions for $\alpha_s = 0.3(0.15)$ shown in Figs. 2b and 3b by the heavy (thin) solid lines are quite similar.

From the plots, we see that in the important region, $\text{Re } \gamma < 0.6$, the resummed NLL BFKL intercept is very similar to that for the DGLAP case. In fact for $\gamma \sim 0.3$ the NLL BFKL value is even a little below the DGLAP intercept. However for large values of $\gamma \gtrsim 0.6$, the NLL BFKL curves go above the DGLAP curves, due an additional positive term from the pole $1/(1 - \gamma + \omega)$ which arises from the inverse k_t -ordered contribution. The approximate equality of the NLL BFKL and DGLAP curves for $\gamma < 0.6$ occurs because this positive contribution is compensated by the virtual corrections corresponding to gluon Reggeization, that is by the higher-twist poles at $\gamma = -1, -2, \dots$ and $\gamma = 2 + \omega, 3 + \omega, \dots$, which give a negative contribution.

As we go into the complex γ plane, the resummed intercept decreases faster than that of DGLAP, and is closer to the original LO BFKL, since we become further away from the twist-2 DGLAP pole at $\gamma = 0$. This decrease of the NLL intercept improves the convergency of the saddle-point integral. To demonstrate this behaviour of ω_s in the complex γ plane, we plot in Figs. 2d and 3d the results for $\text{Im } \gamma = 0.5$. The value of the intercept decreases with increasing $\text{Im } \gamma$ and, due to the higher twist contributions, we indeed see that in the BFKL case it decreases faster than in the DGLAP case.

Finally, we can investigate the role of the quark loop corrections. In Fig. 2 we have considered the (realistic) case of four light quarks ($n_F = 4$). In Fig. 3 we show the analogous results for pure gluodynamics ($n_F = 0$). The inclusion of quark loop contributions evidently shifts the position of the singularity at ω_s to the left; the absolute value of the (negative) virtual quark loop correction is larger than the real quark loop contribution. This demonstrates that the gluon spends part of the ‘evolution time’ (i.e. rapidity interval) in the form of a quark-antiquark state which corresponds to a lower intercept $j < 1$, that is to a negative value of ω_s .

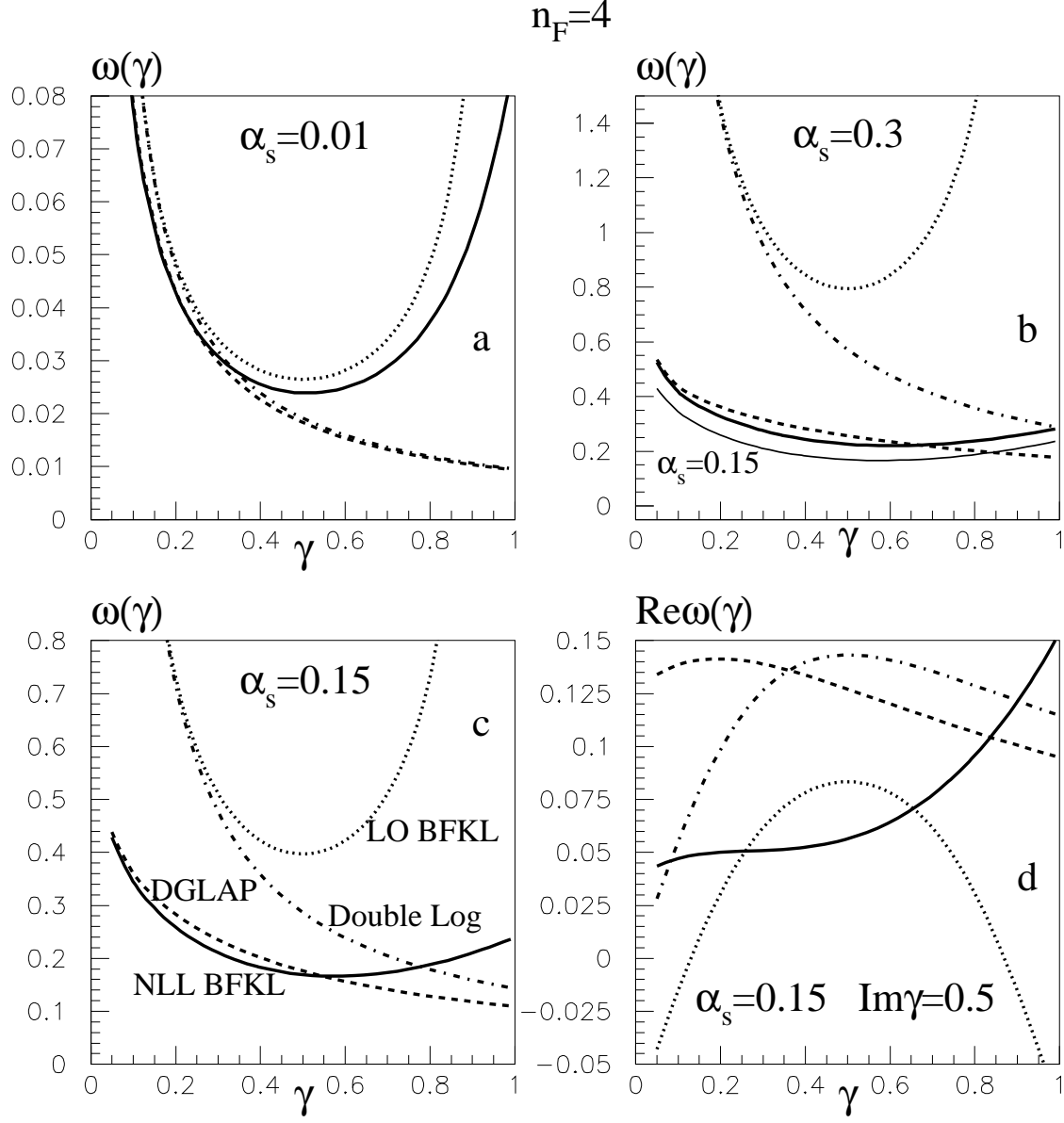


Figure 2: The ‘Pomeron’ intercept, ω_s , obtained by solving Eq. (8), in the following four approximations: LO BFKL; DL; NLL BFKL and LO DGLAP; as described in the text. We include quark-loop corrections, with $n_F = 4$.

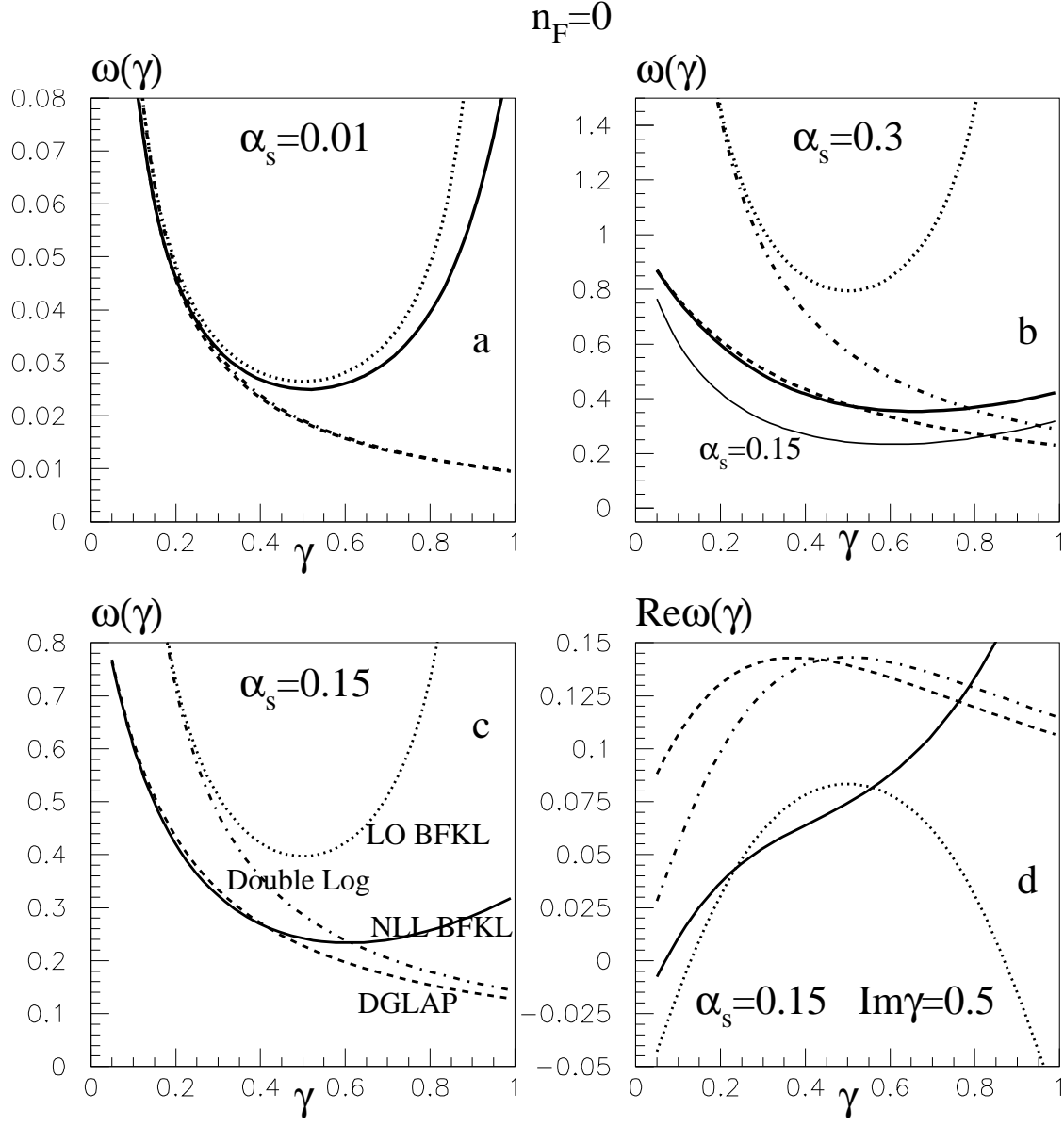


Figure 3: As for Fig. 2, but for pure gluodynamics, with $n_F = 0$.

4 The evolution of the gluon k_t distribution

In this section we use the formalism developed above to study numerically the gluon k_t distribution, and in particular how it changes as one moves along the evolution chain starting from a given input distribution at a particular value of x . We begin by introducing the Green function (G) corresponding to the unintegrated gluon distribution with the initial condition $\delta(1 - k_t^2/k'^2)$ at $x = x'$, i.e. a fixed non-zero value of k_t at $x = x'$. According to the results of the previous section, we have

$$G(r, r'; x, x') = \int_{-i\infty}^{+i\infty} \frac{d\gamma}{2\pi i} e^{\gamma(r-r') + \omega_s(Y-y')}. \quad (18)$$

Here $r' = \ln(k'^2/Q_0^2)$, $y' = \ln(1/x')$ and $\omega_s = \omega_s(\gamma)$ is the solution of (8).

To evaluate the spread in the transverse momentum k'_t at some intermediate value of $y' < Y$ (that is $x' > x$), we write the final unintegrated distribution $f_g(x, k_t)$ as the convolution

$$f_g(x, k_t) = \int \frac{d^2 k'_t}{\pi k_t'^2} f_g(x', k'_t) G(r, r'; x, x') \quad (19)$$

and study the distribution of the integrand over k'_t . It is simplest to elucidate the procedure pictorially. The complete evolution is shown schematically in Fig. 4. We have the source at $x = 1$ and $k_t = Q_0$, and consider the evolution to the final gluon at $x = \exp(-Y)$ and some large value of k_t , say 30 GeV. This point can be reached by different evolution trajectories, indicated by the shaded area in the diagram. Of course the exact form of the shaded region will depend on the approximation used to calculate the behaviour of the gluon along the evolution chain. For example, we shall see that, as expected, LO BFKL with running coupling α_s , tends to populate the low k_t domain much more than the other three approximations that we use.

We are now in a position to study the correlated quantity of experimental interest, that is the distribution of intermediate gluons in a process where a high p_t (or high mass) particle is produced, with (light-cone) momentum fraction $x_+ = x = \exp(-Y)$. The scale of the process specifies the final k_t of our gluon evolution. We have therefore written, in Eq. (19), the final gluon distribution as a convolution in k'_t of the gluon density at x' and the Green function (18) which describes the evolution from x' to the final point x . The quantity of experimental interest is thus the integrand, $f_g(x', k'_t) G(r, r'; x, x')$, which represents the k'_t distribution at an intermediate value of x' . In particular we wish to investigate how the intermediate k'_t distributions, obtained in the various approaches, differ from one another; or, to be more explicit, to see if the NLL BFKL result brings the LO BFKL behaviour close to the DGLAP result. It is convenient to plot the results as the ratio of the integrand to the final gluon density, $f_g(x', k'_t) G(r, r'; x, x') / f_g(x, k_t)$. This corresponds to the ‘normalized’ distribution $k_t'^2 dN/dk_t'^2$ of the intermediate gluons as a function of $\ln k_t'^2$, at the chosen intermediate value $x' = \exp(-y')$.

For the purpose of illustration we calculate the evolution of the gluon k_t distribution taking the initial scale to be $k_t = Q_0 = 1.2$ GeV and choosing the final $k_t = 30$ GeV at $Y = \ln(1/x) = 8$. For the LHC energy ($\sqrt{s} = 14$ TeV) this corresponds to a $E_T = 30$ GeV jet with pseudorapidity $\eta \sim -2$ (in the direction opposite to the parent proton), which can be observed in the central detector. If we set $y' = 4$, we can study the k'_t distribution of the accompanying jets with longitudinal momentum $p_z = E_{\text{beam}} e^{-y'} \sim 55$ GeV (in the parent proton direction).

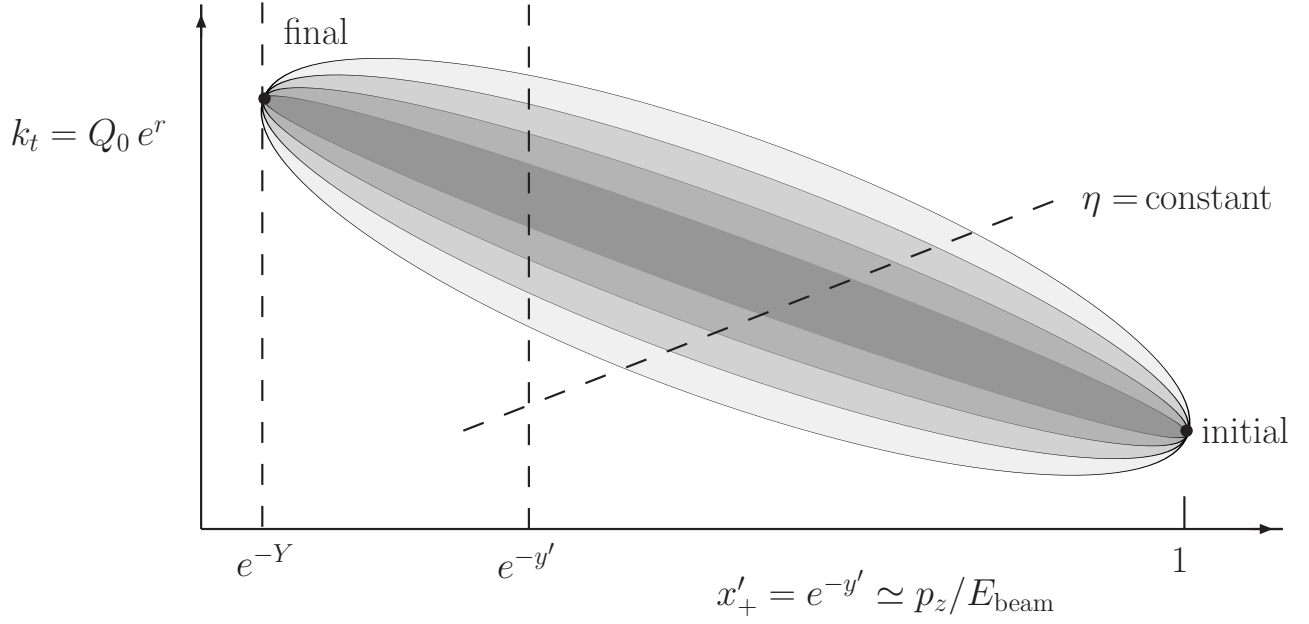


Figure 4: A schematic sketch of the ‘cigar-like’ kinematic domain in x' and k_t covered by the possible paths from the initial to the final evolution points. Note that the scales for k_t and x'_+ are both logarithmic, as indicated by the exponential factors. Also note that the + subscript on x' indicates a light cone variable, which is only introduced to ensure that the fixed η curve is a straight line. Figs. 5 and 6a,b show the gluon k_t distribution at fixed values of y' , whereas Fig. 6c,d show the distributions at fixed η .

The shape of the distribution depends on the initial and boundary conditions. Starting with $f_g = \delta(1 - k_t^2/q_0^2)$ at $x = 1$ (that is from the conditions corresponding to the BFKL Green function) we obtain almost flat distributions (see Fig. 5a) in all four cases: LO BFKL, resummed NLL BFKL, DGLAP and DL. Note that we use the same labelling for the curves as in Figs. 2 and 3. Using instead the input $f_g = \delta(1 - x)$ at $k_t = Q_0$ we obtain distributions that grow almost linearly with $\ln k_t$, see Fig. 5b. This is caused by the boundary condition $f_g(x, k_t = Q_0) = 0$ for any $x < 1$. Again the distributions in all four cases are close to each other.

Next, in Figs. 5c,d we show the results for more realistic input distributions:

$$\text{valence-like } f_g(x, k_t = Q_0) = \sqrt{x}(1 - x)^3 \quad (\text{Fig. 5c}), \quad (20)$$

and

$$\text{Pomeron-like } f_g(x, k_t = Q_0) = x^{-0.1}(1 - x)^3 \quad (\text{Fig. 5d}). \quad (21)$$

All the curves in Fig. 5 are calculated using a fixed $\alpha_s = 0.2$ and $n_F = 0$.

For the valence-like input (20), the initial gluons are concentrated at rather large $x \sim 1$ and the results at low k'_t look qualitatively similar to those in Fig. 5b. For the Pomeron-like input (21) we have a bigger contribution from the small- x and low-scale k_t region. Therefore the distributions are more close to those in Fig. 5a.

To fix the input condition at $k_t = q_0$, the usual procedure for DGLAP evolution, it is easier to work with the ω representation, replacing the contour integration in the γ plane (7) by the integral in the ω plane (10). We have checked that to within a few per cent accuracy both representations give the same function f_g even for the case when we keep only the leading pole in the denominator of the integrand (5). Strictly speaking this can only be true for $n_F = 0$. For a non-zero n_F there is a second pole in the γ plane which corresponds to the second eigenfunction in the singlet DGLAP evolution where we have two equations — one for each of the gluon and quark distributions. In Section 3 we considered the gluon distribution only, and this second (quark) equation reveals itself as a new pole at a γ value comparable with that ($\gamma_s(\omega)$) of the leading pole. To obtain a precise solution we therefore have to keep the contribution from this second pole as well. However in order to simplify the discussion (and computations) in this section, we will consider the case of $n_F = 0$ only.

One advantage of using the representation where we integrate over $d\omega$ is that, as in the DGLAP case, we can include the running of $\alpha_s(k_T'^2)$ simply by replacing the product $\gamma_s(\omega)r$ in the power of the exponent in (18) and (10) by the integral

$$\gamma_s(r - r') \rightarrow \int_{r'}^r \gamma_s(\omega, r'') dr'' \quad (22)$$

where r' is the logarithm of the initial virtuality and the anomalous dimension $\gamma_s(\omega, r'')$ is calculated using the running QCD coupling $\alpha_s(r'')$. Note that in (10) $r' = 0$, of course. The results for running α_s are presented in Fig. 6 for valence-like (20) (Figs. 6a,c) and Pomeron-like (21) (Figs. 6b,d) inputs. In addition to the distributions at $y' = 4$ (that is, at fixed longitudinal momentum $p_z \sim 55$ GeV) which are shown in Figs. 6a,b, we also show, in Figs. 6c,d, the distributions at fixed gluon jet (pseudo)rapidity $\eta' = 2$ in the parent proton direction.

$$Y=8 \quad y'=4 \quad \alpha_s=0.2$$

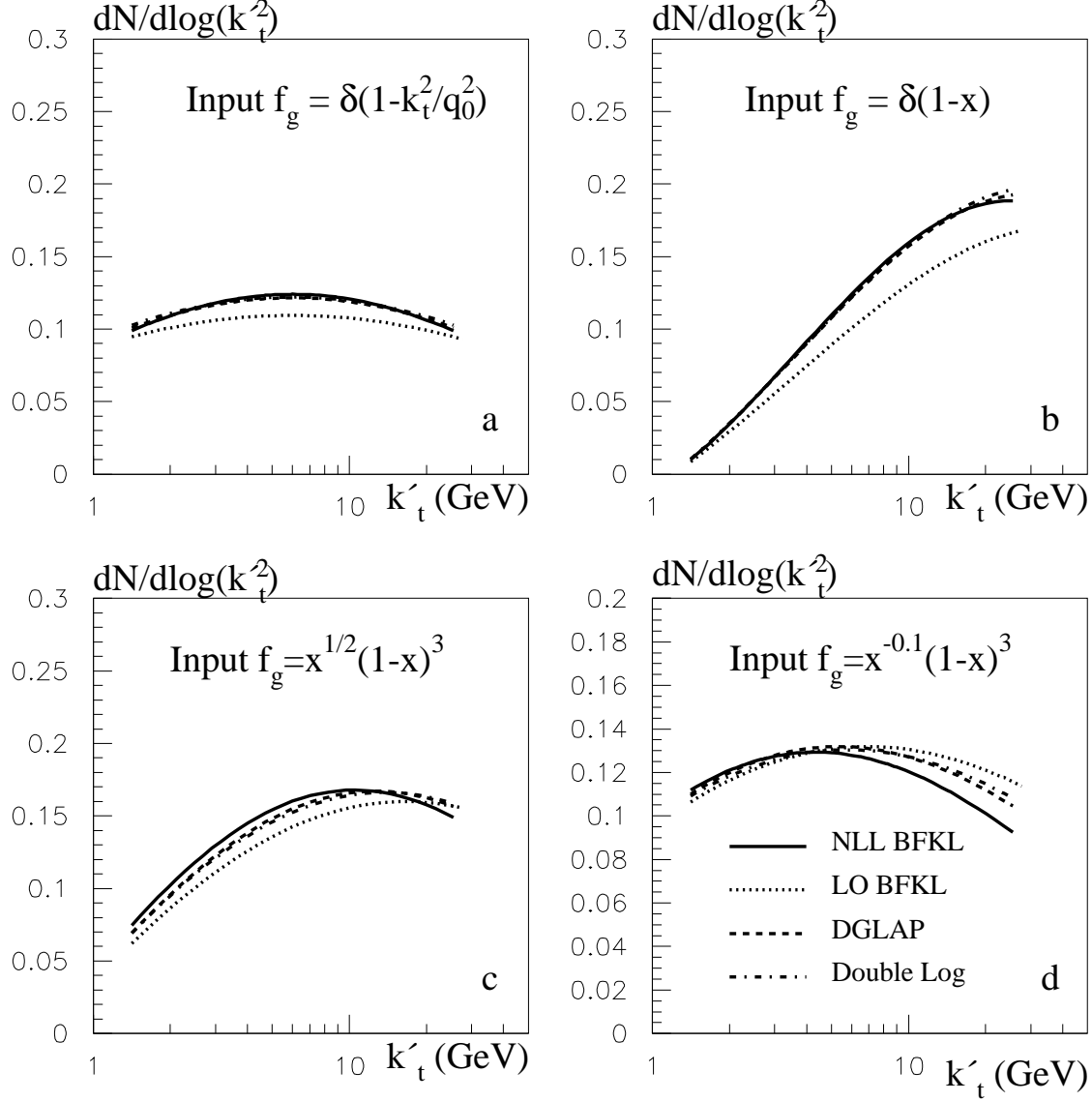


Figure 5: The $k_t'^2 dN/dk_t'^2$ distributions of the intermediate gluons as a function of $\ln k_t'^2$ at intermediate $y' = 4$, for fixed $\alpha_s = 0.2$. We show the four distributions corresponding to using LO BFKL, resummed NLL BFKL, DGLAP and DL, labelled just as in Figs. 2 and 3. The four plots show the distributions for different choices of the input distributions.

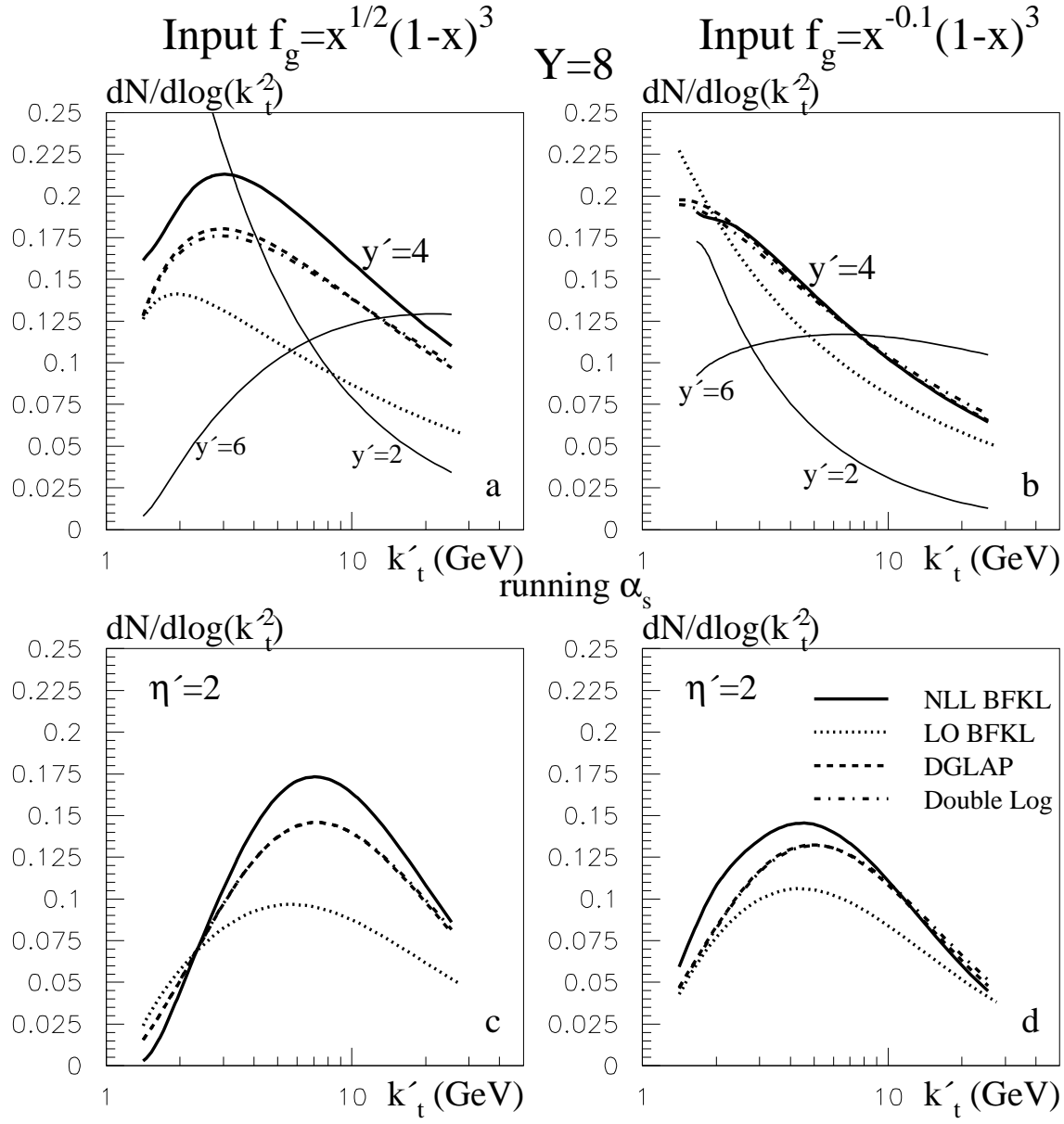


Figure 6: Plots a,b are as for Fig. 5c,d but with running α_s – also shown on these two plots (by thin lines) are the NLL BFKL distributions for the intermediate values $y' = 2$ and 6, as well as the $y' = 4$ distribution which is shown by the thick line. Plots c,d show the gluon distributions for a fixed value of pseudorapidity, $\eta' = 2$, rather than fixed y' .

As expected, including the running α_s shifts the distributions to lower k_t values where the coupling is larger. This is most evident for the LO BFKL curve in Fig. 6b, where the (Pomeron-like) input does not suppress the low k_t region. After the resummation of the NLL corrections, the results depend less on the value of α_s , and the $\ln k_t^2$ distribution of the intermediate gluons becomes broader, with the maximum shifted to a larger k_t in comparison with the LO BFKL distribution. This is a result of the weaker dependence of the resummed intercept on the value of α_s , see Figs. 2 and 3. On the other hand, we see that the form of the NLL k_t' distribution is very similar to that for DGLAP, since the intercepts $\omega(\gamma)$ are almost equal in the region of the saddle points.

In Figs. 6c,d we present the k_t distributions of jets with a fixed pseudorapidity $\eta' = 2$. In this case a small- k_t jet has a smaller longitudinal momentum (that is, a larger $y' = \ln(1/x')$). As k_t increases we therefore move from a distribution with a larger y' to a distribution corresponding to a smaller y' . To illustrate this, we look at the fixed y' plots, Figs. 6a,b, with $y' = 4$. On these plots we also show (by thin lines) the NLL BFKL distributions at two other fixed values, $y' = 2$ and $y' = 6$. It is clear that the distributions at fixed η' have a maximum, since the curves with a larger y' grow with k_t , while for a smaller y' they decrease. In other words, the low k_t domain is suppressed since at fixed η the gluon with a smaller k_t has a smaller longitudinal momentum p_z . In this case the low k_t part of the distribution corresponds to an extreme evolution trajectory, where first the major part of the $\ln(1/x) = Y$ interval is used for BFKL evolution and followed then by an increase due to DGLAP evolution at almost constant x ; see Fig. 4. Of course such evolution trajectories give a much smaller overall contribution than those where both $1/x$ and k_t grow simultaneously leading to double logarithmic $(\alpha_s \ln(1/x) \ln k_t)^n$ contributions.

The effect of inverse k_t -ordering is more evident at fixed η' . For the Pomeron-like input, the NLL distribution is broader than the DGLAP one (see Fig. 6d). However, for valence-like input, it is a bit narrower (see Fig. 6c). The reason is as follows. The cigar-like shape of Fig. 4 is broader for BFKL, so we would anticipate a broader k_t' distribution. However at fixed η' , for low k_t we enter the low x' region where the valence-like input vanishes. This has a larger effect on the more spreadout BFKL distribution than on that of DGLAP, with its thinner cigar which practically does not sample the region with $k_t' \sim Q_0$. Evidently, however, the effect is not very strong and the final NLL BFKL and LO DGLAP distributions do not differ significantly.

This result is of great phenomenological importance, since it implies that for the kinematic regions described above, which are typical of what may be studied at the LHC, parton shower Monte Carlos based on LO DGLAP evolution should give a reasonable approximation to the predictions obtained using a full NLL resummed BFKL calculation.

Recall that the k_t' distributions have been shown in Figs. 5 and 6 in ‘normalized’ form,

$$\frac{dN(x', k_t')}{d\ln k_t'^2} = \frac{f_g(x', k_t') G(r, r'; x, x')}{f_g(x, k_t)}. \quad (23)$$

That is we have shown the density of intermediate gluons with momentum fraction $x' = \exp(-y')$ in events where the final gluon has been detected with momentum k_t and fraction x . Therefore we have introduced the factor $f_g(x, k_t)$ in the denominator. To obtain more insight,

we show, in Fig. 7, the actual k'_t distributions

$$\frac{dF(x', k'_t)}{d\ln k_t'^2} = f_g(x', k'_t)G(r, r'; x, x') \quad (24)$$

obtained in the four approximations, corresponding to Fig. 6b. This quantity, (24), represents the double inclusive cross section – the probability to observe both the final gluon (x, k_t) and the intermediate gluon (x', k'_t) .

5 Determination of the saturation momentum, Q_s

Note that up to now we have been dealing with single ladder graphs and therefore have not taken any account of absorptive corrections (or gluon recombination). These effects are formally suppressed by a factor $1/R^2Q^2$, where $R > 1/Q_0$ is some dimensionful parameter coming from the confinement domain.

However it is well known that at very small x the parton densities grow and the non-linear two- or multi-ladder contributions must eventually become important. This occurs when the cross section for gluon-gluon recombination becomes comparable with the proton area πR^2 , i.e. $\sigma \sim \pi R^2$. Now at high energies the cross section behaves as $\sigma \sim x^{-\omega}/Q^{2(1-\gamma)}$. Therefore to have $\sigma \sim \pi R^2$ requires

$$Q^2 = Q_s^2 \propto x^{-\omega/(1-\gamma)} . \quad (25)$$

This raises the question as to what value of γ (and correspondingly $\omega(\gamma)$) should one use in (25)?

It can be shown that multi-ladder (fan) graphs becomes important for $\gamma > \gamma_c$, where γ_c is given by the equation

$$-\frac{d\omega_s(\gamma_c)}{d\gamma_c} = \frac{\omega_s(\gamma_c)}{1-\gamma_c} . \quad (26)$$

This equation was first obtained in Ref. [15] using the ‘wave front’ method in the framework of the GLR equation. Then it was considered in Ref. [16]. The equation can also be justified on the basis of the Balitsky-Kovchegov equation (in conformal symmetric form) [17, 18]. In the Appendix we show how (26) can be derived using BFKL eigenfunctions.

In order to solve Eq. (25) for γ_c , we return to the γ -integral representation of the amplitude given in Eq. (7). By evaluating the integral using the saddle point method, we see that for large r (i.e. a large interval of $\ln k_t^2$ DGLAP evolution) the value of the saddle point, $\gamma_{\text{sp}} \sim \sqrt{\alpha_s Y/r}$, is small, but increases with the rapidity interval Y . When the position of the saddle point is such that $\gamma_{\text{sp}} < \gamma_c$, the non-linear contributions are negligible. However if $\gamma_{\text{sp}} > \gamma_c$, then the absorptive effects become large and we rapidly reach the saturation regime with $f_g(x, k_t) \propto k_t^2$.

The value of $\gamma_c = 0.37$ was obtained in [15] using the LO BFKL formalism. Evaluating γ_c using the resummed NLL BFKL expressions for ω_s given in Section 2, we arrive at almost the same value — $\gamma_c = 0.32$ for $\alpha_s = 0.3$ — and, in fact, in the limit $\alpha_s \rightarrow 0$ the critical anomalous dimension $\gamma_c \rightarrow 0.37$.

It is straightforward to obtain the x dependence of the saturation momentum $Q_s(x)$. Let us assume that we already reach the value of $Q_s = 1$ GeV at some x_0 . With decreasing x we

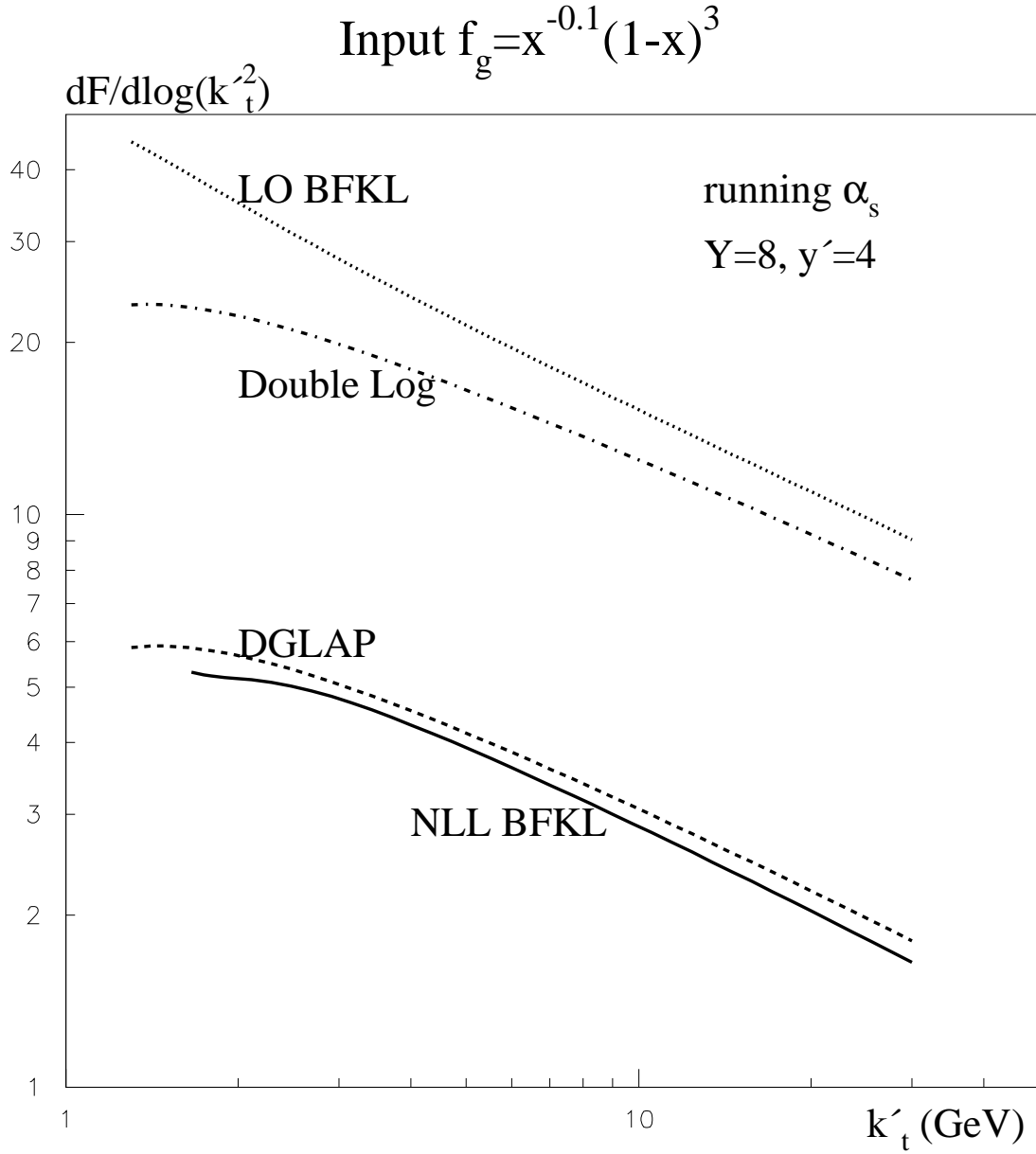


Figure 7: The gluon distributions corresponding to Fig. 6b. Here the intermediate gluon distribution has not been normalized to the probability to find the final gluon with transverse momentum k_t and $x = \exp(-Y)$.

need to increase Q_s in order to keep the saddle point at $\gamma_{\text{sp}} = \gamma_c$. The equation which gives the saddle point of the integration in Eq. (7) is

$$r = \ln Q_s^2 = -Y \frac{d\omega_s}{d\gamma} = Y \frac{\omega_s}{1 - \gamma}, \quad (27)$$

where we have used (26) to get the last equality. We cannot determine the saddle point directly from Eq. (27), since the value of ω_s depends on the running of α_s . Therefore we need to obtain a differential equation. This leads to

$$\frac{d \ln Q_s^2}{d \ln(1/x)} = \frac{\omega_s(\gamma_c)}{1 - \gamma_c}. \quad (28)$$

Solving this equation for γ_c leads to the x dependence of the saturation momentum Q_s that is shown in Fig. 8. Here we include the light quark contribution with $n_F = 4$. The labelling of the various curves is the same as in Fig. 2. We see that after the resummation of the NLL BFKL corrections the value of Q_s grows much more slowly than in the LO BFKL case. Moreover, the NLL BFKL curve even drops below the DGLAP curve, since in the region of $\gamma = 0.3 - 0.4$ the value of

$$\omega_s^{\text{NLL BFKL}} < \omega_s^{\text{DGLAP}}, \quad (29)$$

see Fig. 2. For a low value of α_s , we find the expected ordering

$$Q_s^{\text{LO BFKL}} > Q_s^{\text{NLL BFKL}} > Q_s^{\text{DGLAP}}$$

in Fig. 8b. However at larger values of α_s , we see $Q_s^{\text{NLL BFKL}}$ becomes less than Q_s^{DGLAP} , as shown in Fig 8c,d. Due to the fact that the resummed value of ω_s depends only weakly on α_s , $\ln Q_s^2$ increases almost linearly with $\ln(1/x)$, with

$$Q_s^2 \sim x^{-0.45}. \quad (30)$$

The power of x that we have obtained using NLL resummation is somewhat larger than the result of [19]. Asymptotically, at very large Q_s (and $\alpha_s(Q_s^2) \ll 1$), the LO BFKL (dotted) and the resummed NLL BFKL (solid) curves become parallel.

To determine the saturation momentum, Q_s , from Fig. 8, we need to know the value of x_0 where, by definition, $Q_s = 1$ GeV. If we were to take the model of Ref. [20], then x_0 would be in the range $0.2 \times 10^{-4} - 0.3 \times 10^{-3}$, see Fig. 8 of [20]. If we assume that $x_0 = 10^{-4}$, then we see that the expected saturation region accessible to the experiments at HERA ($Q^2 \sim 2 \text{ GeV}^2$, $x \sim 10^{-5}$) lies outside the pure perturbative domain where one can safely neglect higher-twist effects, power corrections, etc.

6 Conclusions

The k_t distribution of gluons emitted along the gluon chains that accompany a hard subprocess at high energy hadron colliders could give rise to two types of problem. First on the theoretical side, we have the possibility of infrared instability at low k_t . Due to the presence of inverse

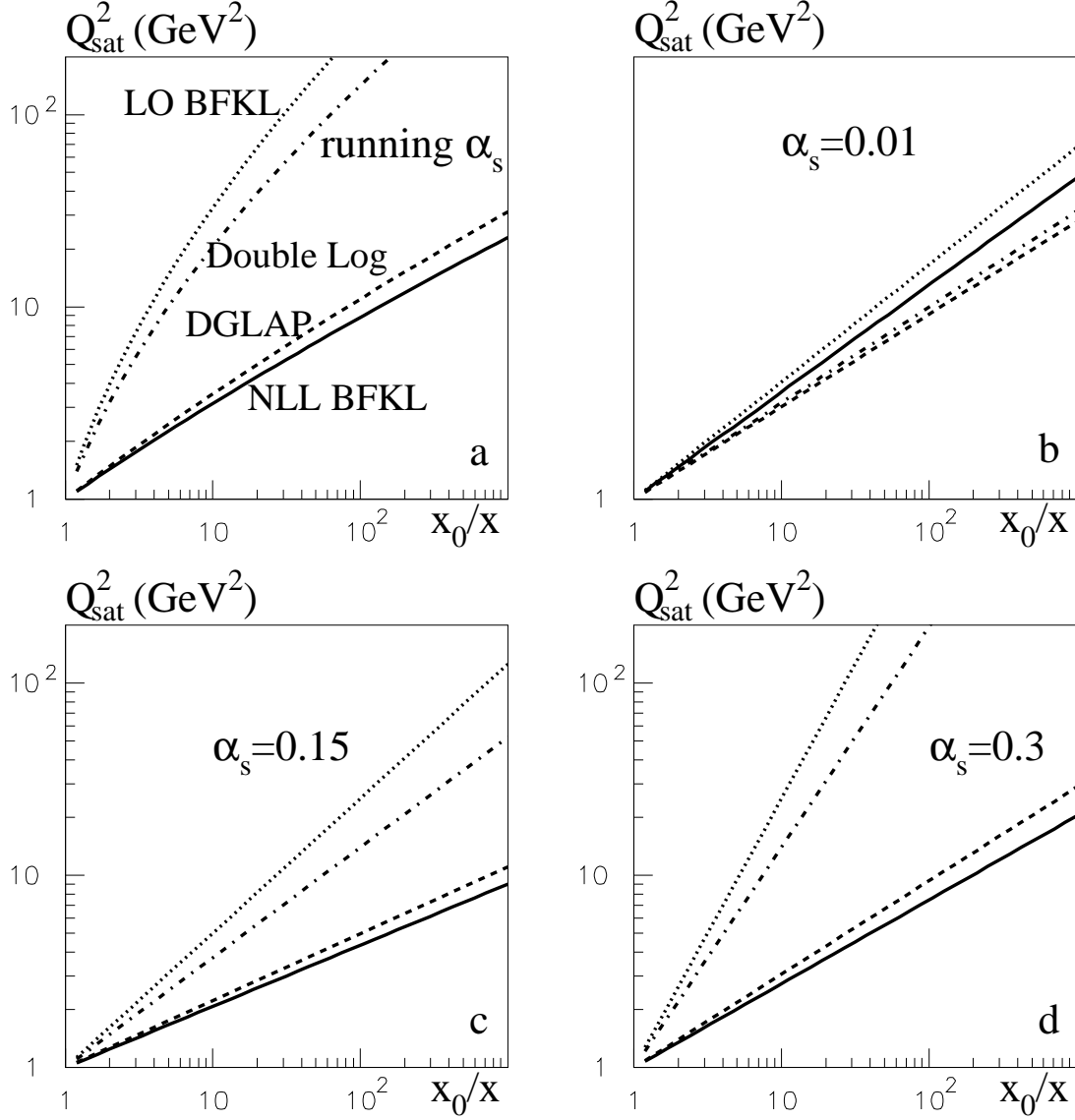


Figure 8: The saturation momentum, Q_s , versus $1/x$. Note that the $1/x$ scale is proportional to x_0 , which, by definition, is the value of x at which $Q_s = 1$ GeV. We discuss in the text that an order of magnitude estimate of x_0 is 10^{-4} .

k_t -ordering, LO BFKL evolution tends to populate the low k_t domain where the QCD coupling α_s is larger. The other potential problem is more experimental. The k_t diffusion, caused by the presence of inverse k_t -ordering, may produce too many large k_t gluons accompanying the hard subprocess, and, as a consequence, obscure the extraction of New Physics.

To study these issues, we have used the prescription of Refs. [8, 9] for NLL BFKL resummation to calculate the resummed BFKL intercept and the k_t distribution of the intermediate gluons emitted during the evolution in both the BFKL and DGLAP cases. We have shown that after such resummation the BFKL intercept becomes much smaller than that obtained using the LO BFKL formalism, and rather close to that obtained using DGLAP evolution. Indeed, the NLL resummation tames both the potential problems. The infrared convergency of the distributions is similar to that for DGLAP. Secondly, for high k_t , the NLL BFKL gluon distribution only slightly exceeds the DGLAP prediction. Thus, contrary to what might be expected from LO BFKL studies, we do not expect any significant increase in accompanying gluon (and therefore minijet and hadron) transverse momentum over and above that which is obtained using the parton shower Monte Carlo approach. It turns out that the presence of the terms with inverse ordering in k_t are approximately compensated by high-twist gluon Reggeization.

Moreover, it follows that the saturation momentum calculated using the resummed NLL BFKL framework is much lower than that predicted by LO BFKL. This implies that we cannot trust the numerical results obtained in the framework of the Balitsky-Kovchegov equation, which is based on LO BFKL. Therefore the growth of the saturation scale Q_s should in practice be much slower than that predicted, for example, in Refs. [21, 22, 23]. Indeed from the NLL BFKL curves in Fig. 8 we conclude that saturation effects are not expected in the pure perturbation region accessible to the experiments at HERA. Even at the LHC, it will not be easy to observe saturation in the perturbative region. Note that, from (30), we have

$$Q_s^2 \simeq 1 \text{ GeV}^2 (x_0/x)^{0.45} = 1 \text{ GeV}^2 (x_0\sqrt{s}/Q_s)^{0.45}. \quad (31)$$

Solving this equation at the LHC energy, $\sqrt{s} = 14 \text{ TeV}$, we obtain in the centre of the pseudo-rapidity plateau

$$Q_s(\eta = 0) \simeq 1 \text{ GeV} (x_0\sqrt{s}/1 \text{ GeV})^{0.18} \simeq 1.1 (1.6) \text{ GeV}, \quad (32)$$

assuming that $x_0 = 10^{-4}$ (10^{-3}). Thus, at the LHC, the only chance to observe saturation phenomena, with the scale not too low, $Q^2 \sim 10 \text{ GeV}^2$ say, is to study processes in the fragmentation region, with $x_- \sim 0.1$ and $x_+ \sim 10^{-6}$.

The k_t distribution of intermediate gluons emitted along the evolution chain depends strongly on the form of the input conditions. For a realistic ‘Pomeron-like’ input the distributions predicted by the resummed NLL BFKL and DGLAP evolutions are rather close to each other. However, because of the contribution of configurations with inverse k_t ordering the NLL BFKL distribution is slightly wider (i.e. has a larger dispersion).

Acknowledgements

We thank Gavin Salam for stimulating this study and for fruitful discussions. ADM thanks the Leverhulme Trust for an Emeritus Fellowship and MGR thanks the IPPP at the University of Durham for hospitality. This work was supported by the UK Particle Physics and Astronomy Research Council, by a Royal Society special project grant with the FSU, by grant RFBR 04-02-16073 and by the Federal Program of the Russian Ministry of Industry, Science and Technology SS-1124.2003.2.

Appendix: equation for the critical anomalous dimension,

γ_c

The non-linear BFKL evolution equation is⁶

$$\frac{df_g(x, k_t)}{dY} = \int dk_t'^2 K(k_t, k_t') f_g(x, k_t') - \int dk_t'^2 V \cdot f_g^2(x, k_t') \quad (33)$$

where $K(k_t, k_t')$ is the BFKL kernel and V is the triple Pomeron vertex. If we expand the amplitude in terms of the conformal eigenfunctions $E_\gamma = e^{\gamma r}$ (for the case of our forward amplitude with $n = 0$),

$$f_g = \int e^{\gamma r} F(\gamma, Y) d\gamma, \quad (34)$$

then we obtain the following equation for $F(\gamma, Y)$

$$\frac{dF(\gamma, Y)}{dY} = \omega_s(\gamma) F(\gamma, Y) - \int \int v \cdot F(\gamma_1, Y) F(\gamma_2, Y) d\gamma_1 d\gamma_2, \quad (35)$$

where $Y = \ln(1/x)$, and where the triple pomeron vertex in the γ representation is denoted by v . In addition to the extra α_s (in comparison with ω_s), the vertex V contains the factor $1/R^2 Q^2 = 1/R^2 k_t^2$, which represents the small probability of recombination of two gluons of size $\sim 1/k_t$ homogeneously distributed over a domain of transverse size $\sim R$. When going from Eq. (33) to Eq. (35), we have integrated the product of the vertex V and the two eigenfunctions E_{γ_1} and E_{γ_2} (hidden in f_g) over the transverse momentum k_t' . The integral over dk_t' gives a pole $1/(1 + \gamma - \gamma_1 - \gamma_2)$ which reflects the conservation law for the anomalous dimensions. One of the integrals, say $d\gamma_1$, may be done by closing the contour on this pole, while the other ($d\gamma_2$) can be performed by the saddle point method. Because of the symmetry of the expression, the saddle point gives $\gamma_1 = \gamma_2$. Thus Eq. (35) takes the form

$$\frac{dF(k, Y)}{dY} = \omega_s(k) F(k, Y) - \bar{v} F^2(k/2, Y), \quad (36)$$

⁶Here we neglect the dependence on the momentum transferred through the amplitude and consider only the component with zero conformal spin $n = 0$ (that is, we consider the forward amplitude with a flat azimuthal dependence). Recall that the eigenfunctions which have $n \neq 0$ correspond to $\omega_s < 0$ [1] and therefore the non-linear contribution with $n \neq 0$ will in any case be small, being suppressed by at least a factor α_s , in comparison with the linear one.

where the variables γ and γ_i are related to the ‘wave vector’[15] k by

$$\gamma = 1 - k \quad (37)$$

$$\gamma_1 = \gamma_2 = \frac{1 + \gamma}{2} = 1 - \frac{k}{2}. \quad (38)$$

In Eq. (36), \bar{v} now denotes the triple Pomeron vertex together with the measure of integration around the saddle point.

To solve (36) we use the method of characteristics. In the stationary case, $dF/dY = 0$, we have

$$\omega_s(k)F(k, Y) = \bar{v}F^2(k/2, Y). \quad (39)$$

The solution of (39) may be written as $F = a(k, Y)e^{fkY}$ where the factor f in the power of the exponent can be found by matching the function $F(k, Y)$ in the region of non-linear and linear evolution, neglecting the non-linear term in the latter. In the linear case $fk = \omega_s(k)$. Matching the first derivative⁷, we obtain Eq. (26),

$$d(fk)/dk = f = \omega_s/k = d\omega_s(k)/dk, \quad (40)$$

where, recall, $k = 1 - \gamma$.

References

- [1] L.N. Lipatov, Sov. J. Nucl. Phys. **23** (1976) 338;
V.S. Fadin, E.A. Kuraev and L.N. Lipatov, Phys. Lett. **B60** (1975) 50;
V.S. Fadin, E.A. Kuraev and L.N. Lipatov, Sov. Phys. JETP **44** (1976) 443;
V.S. Fadin, E.A. Kuraev and L.N. Lipatov, Sov. Phys. JETP **45** (1977) 199;
I.I. Balitsky and L.N. Lipatov, Sov. J. Nucl. Phys. **28** (1978) 822, JETP Lett. **30** (1979) 355.
- [2] M. Ciafaloni, Nucl. Phys. **B296** (1988) 49;
S. Catani, F. Fiorani and G. Marchesini, Phys. Lett. **B234** (1990) 339; Nucl. Phys. **B336** (1990) 18;
G. Marchesini, Nucl. Phys. **B445** (1995) 49.
- [3] V.S. Fadin and L.N. Lipatov, Phys. Lett. **B429** (1998) 127
G. Camici and M. Ciafaloni, Phys. Lett. **B430** (1998) 349.
- [4] J.P. Andersen and A. Sabio Vera, Phys. Lett. **B567** (2003) 116; Nucl. Phys. **B679** (2004) 345.
- [5] M. Ciafaloni, D. Colferai, G.P. Salam and A.M. Stasto, Phys. Rev. **D68** (2003) 114003.
- [6] S.J. Brodsky, V.S. Fadin, V.T. Kim, L.N. Lipatov and G.B. Pivovarov, JETP Lett. **70** (1999) 155.

⁷Second and higher derivatives can be matched by an appropriate choice of the pre-exponent factor $a(k, Y)$.

- [7] G.P. Salam, talk presented at the IPPP Workshop on TeV-Scale Physics, Cambridge, England, July 2002, ‘Small-x (a micro review)’, www.lpthe.jussieu.fr/~salam/talks/
- [8] G.P. Salam, JHEP **9807** (1998) 019;
M. Ciafaloni, D. Colferai and G.P. Salam, Phys. Lett. **B452** (1999) 372; Phys. Rev. **D60** (1999) 114036.
- [9] G.P. Salam, Acta Phys. Pol. **B30** (1999) 3679.
- [10] E.M. Levin, G. Marchesini, M.G. Ryskin and B.R. Webber, Nucl. Phys. **B357** (1991) 167.
- [11] G. Altarelli, R.D. Ball and S. Forte, Nucl. Phys. **B674** (2003) 459.
- [12] M.A. Kimber, A.D. Martin and M.G. Ryskin, Phys. Rev. **D63** (2001) 114027;
G. Watt, A.D. Martin and M.G. Ryskin, Eur. Phys. J. **C31** (2003) 73.
- [13] A.D. Martin, R.G Roberts, W.J. Stirling and R.S. Thorne, Eur. Phys. J. **C35** (2004) 325.
- [14] R.K. Ellis, Z. Kunszt and E.M. Levin, Nucl. Phys. **B420** (1994) 517, erratum-ibid. **B433** (1995) 498.
- [15] L.V. Gribov, E.M. Levin and M.G. Ryskin, Phys. Rep. **100** (1983) 1.
- [16] J. Bartels and E.M. Levin, Nucl. Phys. **B387** (1992) 617.
- [17] J. Bartels, G.P. Vacca and M.G. Ryskin, in preparation.
- [18] S. Munier and R. Peschanski, Phys. Rev. **D69** (2004) 034008.
- [19] D.N. Triantafyllopoulos, Nucl. Phys. **B648** (2003) 293.
- [20] J. Bartels, K. Golec-Biernat and H. Kowalski, Phys. Rev. **D66** (2002) 014001.
- [21] E. Levin and M. Lublinsky, Nucl. Phys. **A696** (2001) 833.
- [22] E. Gotsman, M. Kozlov, E. Levin, U. Maor and E. Naftali, hep-ph/0401021.
- [23] E. Iancu, K. Itakura and L. McLerran, Nucl. Phys. **A708** (2002) 327.